https://doi.org/10.5194/egusphere-2025-447
Preprint. Discussion started: 13 February 2025

Reviews and syntheses: Potential and limitations of oceanic carbon dioxide storage via reactor-based accelerated weathering of limestone

Tom Huysmans[1], Filip J. R. Meysman[1], Sebastiaan J. van de Velde[2,3,1]

[1] Department of Biology, University of Antwerp, Wilrijk, 2610, Belgium
[2] Department of Marine Science, University of Otago, Dunedin, 9016, New-Zealand
[3] National Institute of Water and Atmospheric Research, Wellington, 6022, New-Zealand

Correspondence to: Tom Huysmans (tom.huysmans@uantwerpen.be)

Abstract. To achieve climate stabilization, substantial emission reductions are needed. Emissions from industrial point sources can be reduced by applying carbon capture and storage (CCS) methods, which capture carbon dioxide (CO_2) before it is released to the atmosphere. CCS applications typically target CO_2 storage within geological reservoirs. Accelerated weathering of limestone (AWL) provides an alternative CCS approach, in which CO_2 is stored as dissolved inorganic carbon in the ocean. At present, AWL technology remains at the pilot scale with no industrial implementation. Here, we review the proposed reactor designs for AWL, comparing them in terms of CO_2 capture efficiency, $CaCO_3$ dissolution efficiency, CO_2 sequestration efficiency, and water usage. For this, we represent AWL as a four step process: (i) CO_2 dissolution, (ii) $CaCO_3$ dissolution, (iii) alkalinization (step only included in the case of buffered AWL), and lastly (iv) re-equilibration. AWL application is generally characterized by a large water usage and the need for large reactor sizes. Unbuffered AWL approaches show substantial degassing of CO_2 back to the atmosphere after the process water is discharged. Buffered AWL compensates the unreacted CO_2 by $Ca(OH)_2$ addition, and hence prevents degassing, which substantially increases the CO_2 sequestration efficiency. Yet, buffered AWL require a source of CO_2-neutral $Ca(OH)_2$. The need for process water can be reduced by increasing the CO_2 fraction of the gas stream or increasing its pressure. Further optimization of the pulverized carbonate particles could reduce the amount of $Ca(OH)_2$ needed to buffer the unreacted CO_2. The anticipated CO_2 sequestration efficiency of buffered AWL is comparable with that projected for large-scale CCS in geological reservoirs.

1. Introduction

Atmospheric CO_2 levels have increased by ~50 % compared to preindustrial times and are higher than any period in the past two million years (Calvin et al., 2023). The 2015 Paris climate agreement aims to prevent global temperatures from rising more than 2 °C compared to preindustrial levels (Sanderson et al., 2016). To this end, climate policies are focused on the reduction of greenhouse gas (GHG) emissions, which involves reduced usage of fossil fuels, in conjunction with the development of Carbon Capture and Storage (CCS) methods. To provide a timely and meaningful contribution to climate mitigation, these CCS technologies need to be implemented at the Gigaton scale within the next decade, which requires a strong acceleration of their development (United Nations Environment Programme, 2024).

One of the proposed technologies to achieve CCS from point-source CO_2 emissions is "enhanced rock weathering", which aims to accelerate the natural process of chemical weathering of silicate and carbonate rocks (Rau and Caldeira, 1999; Renforth and Kruger, 2013; Caserini et al., 2021). This targeted weathering process can take place *in situ*, in which CO_2 is first captured from the flue gas and then injected into suitable silicate rock formations (basalts and ultramafic rocks). The CO_2 is then trapped by a carbonation reaction with the ambient silicate rock, thus ensuring a permanent, geological storage (Matter and Kelemen, 2009; Romanov et al., 2015; Gadikota, 2021; Cao et al., 2024). However, there are certain geomechanical risks associated with geological storage of CO_2, such as CO_2 leakage, induced seismicity, the loss of well integrity and surface uplift (Song et al., 2023). Moreover, suitable rock formations for storage are not always in close proximity to the CO_2-emitting installations, thus requiring compression and transport of CO_2.

Alternatively, the chemical weathering can also be executed under controlled conditions in a land-based reactor, close to the industrial point source. CCS via such reactor-based enhanced rock weathering can follow two main approaches, depending on whether silicates are used as feedstock material (usually referred to a "*ex situ* mineral carbonation" technologies; Romanov et al., 2015; Gadikota, 2021) or whether carbonates are used as weathering substrates (referred to a as "accelerated weathering of limestone"; Rau and Caldeira, 1999). In *ex situ* mineral carbonation (ESMC), a finely grounded silicate mineral (e.g. olivine Mg_2SiO_4) is fed into a reactor, where it reacts at elevated temperature and pressure with CO_2 from a flue gas to eventually form stable carbonates (e.g. magnesite Mg_2SiO_4) - see recent reviews (Snæbjörnsdóttir et al., 2020; Veetil and Hitch, 2020; Thonemann et al., 2022). Alternatively, during the accelerated weathering of limestone (AWL), CO_2 is stripped from the flue gas using a mixture of seawater and limestone ($CaCO_3$) (Rau and Caldeira, 1999; Renforth and Henderson, 2017), and the resulting effluent is discharged into the sea.

The main difference between the two approaches is that ESMC stores CO_2 in a mineral form, whereas AWL stores CO_2 in dissolved form in the ocean. As such, AWL bears similarities with so-called ocean alkalinization approaches, which target the deliberate removal of CO_2, by increasing the alkalinity (A_T) of the surface ocean (Kheshgi, 1995; Meysman and Montserrat, 2017; Renforth and Henderson, 2017). Natural chemical weathering of silicate and carbonate rocks generates alkalinity (A_T) (Berner and Berner, 2004), which is transported by rivers to the ocean. Increasing seawater A_T, which is defined as the excess of base (proton acceptors) over acid (proton donors) (Dickson, 1981; Zeebe and Wolf-Gladrow, 2001), shifts the carbonate equilibrium away from dissolved CO_2 towards bicarbonate (HCO_3^-) and carbonate (CO_3^{2-}) ions. As a result, more atmospheric CO_2 can be stored in seawater as dissolved inorganic carbon (DIC; defined as the sum of the aqueous [CO_2], [HCO_3^-] and [CO_3^{2-}]

concentrations; Zeebe and Wolf-Gladrow, 2001). This natural process of ocean alkalinization has regulated atmospheric CO_2 and stabilized the climate over geological time scales (Berner et al., 1983). The process of AWL aims to mimic the natural process of carbonate weathering in a reactor, but in an accelerated fashion. Here, we review the potential of AWL as a CCS approach, including its intricacies and possible bottlenecks. To this end, we describe AWL thermodynamically as a four step process, thus providing a model framework that allows to calculate the efficiency of the different steps as well as the overall CO_2 sequestration potential. We then review the different reactor designs that have been proposed for the AWL process in recent years, and evaluate their efficiency and potential in terms of CCS capacity.

2. The theoretical principle of AWL

2.1. AWL as a four-step process

The concept of AWL was first proposed by Rau and Caldeira more than two decades ago (Rau and Caldeira, 1999). It provides a geochemistry-based method for CCS in which the dissolution of carbonate minerals is artificially enhanced (Rau and Caldeira, 1999). Finely ground carbonate (e.g., calcite, aragonite, dolomite or magnesite) and a suitable stream of process water are brought into direct contact with the flue gasses from a CO_2-intensive industrial source, such as a coal-fired power plant or a cement factory (Fig. 1). In general, the process of AWL can be described as consisting out of four different steps (Fig. 1): (i) **CO_2 uptake**: the process water comes into contact with the flue gas, which has a much higher partial pressure of CO_2 (typically $pCO_2 \approx 0.15$ atm). This leads to dissolution of CO_2 in the process water, thus increasing the dissolved inorganic carbon (DIC), and lowering the pH and saturation state (Ω_{calc}), while keeping A_T constant; (ii) **$CaCO_3$ dissolution**: the reduced saturation state (Ω_{calc}) of the process water stimulates the dissolution of carbonate particles and increases both the DIC and A_T of the process water. Subsequently, there are two options. In the case of 'buffered AWL" , there is an additional **(iii) alkalinization step** before re-equilibration to avoid the degassing of CO_2. Additional alkalinity is added to the process water (e,g. by lime addition) until the excess CO_2 is fully buffered. Upon discharge, there is no longer any CO_2 transfer to the atmosphere. In the case of 'unbuffered AWL", there is the **(iv) re-equilibration step**: the process water is discharged into the sea without any further treatment. Upon discharge, the process water re-equilibrates with the atmosphere at the lower pCO_2 ($pCO_2 \approx 0.00042$ atm), and the excess CO_2 (i.e., the part of DIC not stabilized by the increased alkalinity) will degas back to the atmosphere.

Below we discuss each step in more detail. During the whole AWL process, the process water goes through four consecutive states, each characterized by a specific set of A_T, DIC, pCO_2, and pH values: (1) the ambient process water that is used as intake, (2) the process water with elevated DIC after CO_2 uptake, (3) the process water enriched in A_T and DIC after $CaCO_3$ dissolution, (4a-b) the unbuffered or buffered process water upon discharge.

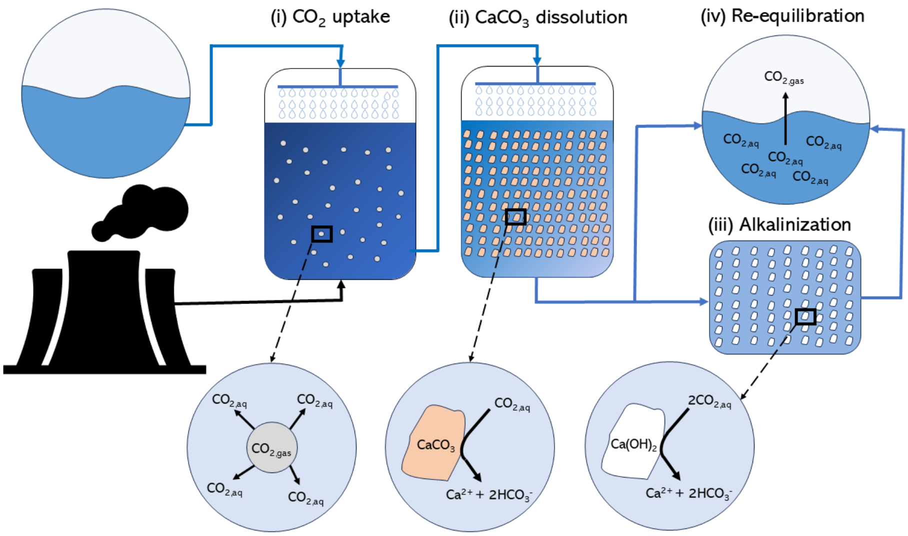

Figure 1. The process of accelerated weathering of limestone can be described by four different steps: (i) CO_2 uptake: CO_2 from the flue gas comes in contact with the process water and CO_2 dissolves into the process water, (ii) $CaCO_3$ dissolution: Aqueous CO_2 reacts with $CaCO_3$ particles and generates A_T in the form of HCO_3^-, which is stimulated by the reduced saturation state, (iii) the alkalinization step (in buffered AWL): Additional alkalinity is added to the process water (e,g. by lime addition), until the excess CO_2 is fully buffered, and (iv) the re-equilibration step: Upon re-exposure to atmospheric conditions, aqueous CO_2 which is not stabilized by the increased A_T will degas back to the atmosphere. The black lines indicate the gas flows and the blue lines indicate the process water flows.

Table 1 shows the values for pCO_2, A_T, DIC, pH and Ω_{calc} in each of the four states for a representative case study, which is based on data reported from a two-step pilot reactor consisting of a separate gas-liquid and liquid-solid reactor (see Chou et al., 2015, and as further discussed below). The CO_2 concentration of the gas stream was 15%, while the pCO2 of the atmosphere is fixed at 420 ppm. The A_T and DIC values at the inlet and outlet of the reactor are based on measured values (Table 1). The remaining variables are calculated using the CRAN:AquaEnv package for the thermodynamic equilibria of acid-base systems in seawater (Hofmann et al., 2010). We assume full re-equilibration with the atmosphere (unbuffered AWL) or full buffering with $Ca(OH)_2$ upon discharge into the sea (buffered AWL). The transition through the different consecutive states is depicted in the thermodynamic diagrams of Fig. 2, which each plot depicting the gas phase pCO_2 versus the process water A_T, but with different isolines (DIC, pH and Ω_{calc}).

Table 1. Theoretical values for alkalinity (A_T), dissolved inorganic carbon (DIC), pH and calcite saturation state (Ω_{calc}) in the four consecutive states of the example AWL reactor. ΔDIC_{seq} is the DIC that is added to the process water due to dissolution from the gas stream and ΔDIC_{carb} is the DIC added through the dissolution of $CaCO_3$. The pCO_2, A_T and DIC values (indicated by #) are based on values measured in a two-step AWL pilot reactor (Chou et al., 2015). The values of A_T, DIC, pH, and Ω_{calc} (indicated with *) are calculated using CRAN:AquaEnv (Hofmann et al., 2010) for seawater at a temperature of 15 °C and salinity of 35.

State	pCO_2 (atm)	A_T (mM)	DIC (mM)	ΔDIC_{seq} (mM)	ΔDIC_{carb} (mM)	pH (-)	Ω_{calc} (-)
(1)	0.000420	$2.26^{\#}$	$2.13^{\#}$	0	0	7.93^{*}	2.50^{*}
(2)	$0.15^{\#}$	2.26	2.96^{*}	0.83	0	6.52^{*}	0.110^{*}
(3)	0.15	$2.64^{\#}$	$3.15^{\#}$	0.83	0.19	6.72^{*}	0.203^{*}
(4a)	0.000420	2.64	2.38^{*}	0.06	0.19	8.16^{*}	4.62^{*}
(4b)	0.000420	3.56^{*}	3.15^{*}	0.83	0.19	8.27^{*}	7.74^{*}

During step (i), the alkalinity remains invariant between state (1) and state (2) (vertical trajectory in Fig. 2). The high CO_2 concentration in the flue gas drives the dissolution of CO_2 into the water phase, which increases the DIC of the process water (Fig. 2a), lowers its pH (Fig. 2b) and drastically lowers the calcite saturation state ($\Omega_{calcite}$) (Fig. 2c; Table 1). As a result, the dissolution of carbonate minerals in step (ii) becomes thermodynamically favorable, and because of the strong disequilibrium, the dissolution rate is increased (Berner and Morse, 1974; Morse et al., 2007).

$$CO_2 + H_2O + CaCO_3 \rightarrow Ca^{2+} + 2HCO_3^- \tag{1}$$

Because the input of A_T from carbonate dissolution is twice that of DIC, the carbonate equilibrium in the process water is shifted away from CO_2 towards HCO_3^- and CO_3^{2-} (Eq. 2), which slightly increases the pH and calcite saturation state (Fig. 2; Table 1).

$$H_2O + CO_2 \leftrightarrow HCO_3^- + H^+ \leftrightarrow CO_3^{2-} + H^+ \tag{2}$$

In the unbuffered AWL scenario, the effluent water of the reactor is simply discharged in the marine environment and is re-exposed to the atmosphere. We can model this as a re-equilibration of the process water with the ambient atmospheric pCO_2, step (iv), which will induce an outgassing of excess dissolved CO_2. The release of CO_2 from the effluent results in a marked decrease of DIC, and a concomitant increase in pH and Ω_{calc} (Fig. 2; Table 1).

Two assumptions are worth noting. In the calculation above, we assumed that the effluent process water first equilibrates with the ambient atmosphere, before it is mixed with the surrounding seawater. In reality, the process water will be mixed first with ambient seawater. However, one can easily show that equilibration followed by mixing, provides the same CO_2 transfer as mixing followed by equilibration. Secondly, the calcite saturation state of the solution after degassing is larger than one, and such a supersaturated solution could (at least in theory) induce the reprecipitation of $CaCO_3$ within the marine environment with a resulting loss of A_T. Still, the abiotic precipitation of $CaCO_3$ in seawater typically requires a highly supersaturated solution ($\Omega_{calc} > 18$) (Morse and He, 1993), and therefore abiotic $CaCO_3$ formation is unfavorable and rare under natural conditions (Mucci et al., 1989). Accordingly, we assume that no carbonate precipitation takes place after the discharge of the process water.

In the buffered AWL scenario, $Ca(OH)_2$ is added to the process water before its discharge into the marine environment (Caserini et al., 2021). During this step, all the unreacted CO_2 is buffered, which hence prevents any loss of DIC (Fig 2a), increases alkalinity and pH, and also substantially increases Ω_{calc} ~8 (Fig. 2b-c). The abiotic precipitation of $CaCO_3$ under high Ω_{calc} values could be circumvented by discharging the process water where: 1) rapid mixing and dilution occurs, 2) mixing with deeper and colder waters, which increases the solubility of carbonates, or 3) a direct injection of the process at a depth below the calcite compensation depth (Kirchner et al., 2020a).

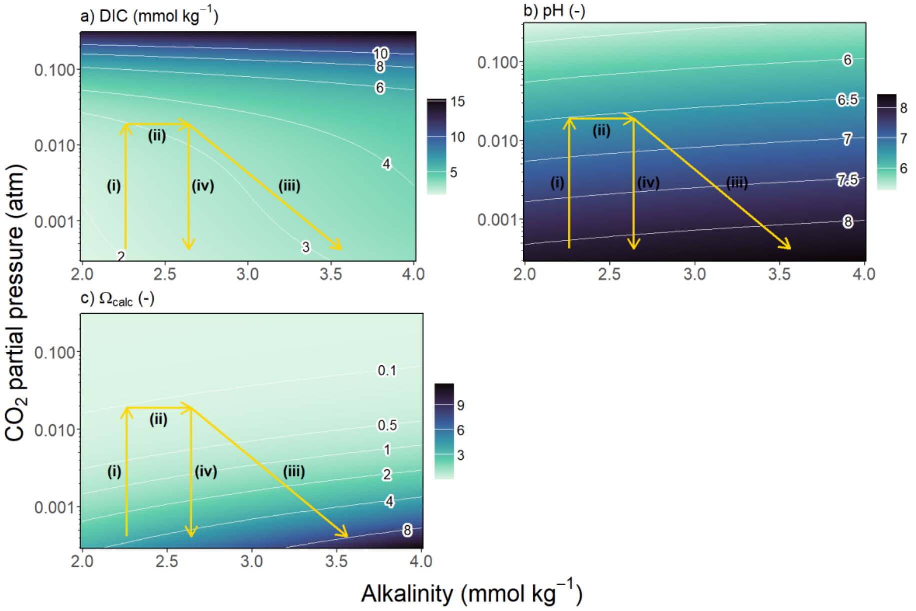

Figure 2. Changes in carbonate chemistry for the four different steps during AWL: (i) CO_2 uptake: CO_2 gas from the flue gas comes in contact with the process water and CO_2 dissolves into the process water, (ii) $CaCO_3$ dissolution: Aqueous CO_2 reacts with $CaCO_3$ particles and generates A_T in the form of HCO_3^-, which is stimulated by the reduced saturation state, (iii) the alkalinization step (in buffered AWL): Additional alkalinity is added to the process water (e,g. by lime addition), until the excess CO_2 is fully buffered and (iv) the re-equilibration step: Upon re-exposure to atmospheric conditions, aqueous CO_2 which is not stabilized by the increased A_T will degas back to the atmosphere. pCO_2 (atm) in function of alkalinity (mmol kg^{-1}) with isolines for a) DIC, b) pH and c) calcite saturation state (Ω_{calc}). The DIC concentration in the process water has increased over the course of the three consecutive steps indicating a capture of CO_2.

2.2. CO_2 sequestration during carbonate dissolution and lime buffering

Overall, the A_T increase following carbonate dissolution leads to the sequestration of CO_2 from the flue-gas in the form of DIC in the seawater (Rau and Caldeira, 1999; Caldeira and Rau, 2000; Rau et al., 2007; Rau, 2011). As can be seen from Table 1, the final DIC (2.38 mM in the unbuffered case; 3.15 mM in the buffered case) is higher than in the intake water (2.13 mM). However, only part of this DIC increase is due to CO_2 sequestration from the flue gas, as part of the additional DIC also originates from $CaCO_3$ dissolution. To separate the different effects that contribute to CO_2 sequestration, the DIC increase can be decomposed as:

$$\Delta DIC_{total} \equiv DIC_{final} - DIC_{inlet} = \Delta DIC_{seq}^{unbuf} + \Delta DIC_{seq}^{buf} + \Delta DIC_{carb} \tag{3}$$

DIC_{inlet} is the DIC value measured in the process water at the inlet, ΔDIC_{carb} denotes the DIC that originates from $CaCO_3$ during dissolution, ΔDIC_{seq}^{unbuf} represents the DIC in the process water that originates from net CO_2 sequestration from the flue gas in the reactor and ΔDIC_{seq}^{buf} represents the DIC that is retained (i.e. prevented from efflux to the atmosphere) due to the lime buffering of the effluent (in the unbuffered scenario $\Delta DIC_{seq}^{buf} = 0$). In a similar fashion, the final alkalinity value is the result of alkalinity addition during carbonate dissolution and possibly some extra addition during lime buffering

$$\Delta A_{T,total} \equiv A_{T,final} - A_{T,inlet} = \Delta A_{T,carb} + \Delta A_{T,buf} \tag{4}$$

From this, the net CO_2 sequestration is obtained by subtraction of the DIC that originates from $CaCO_3$ dissolution:

$$\Delta DIC_{seq} \equiv \Delta DIC_{seq}^{unbuf} + \Delta DIC_{seq}^{buf} = \Delta DIC_{total} - \Delta DIC_{carb} \tag{5}$$

In practical AWL applications, the Δ quantities can be determined by measuring DIC and A_T at the inlet and outlet of the AWL reactor (i.e., before the buffering step), complemented by thermodynamic calculations (see Table 1). The DIC and A_T increase due to carbonate dissolution can be directly inferred from the stoichiometry of the $CaCO_3$ dissolution reaction Eq. (1) :

$$\Delta A_{T,carb} = A_{T,outlet} - A_{T,inlet} \,, \quad \Delta DIC_{carb} = \frac{A_{T,outlet} - A_{T,inlet}}{2} = \frac{1}{2}\Delta A_{T,carb} \tag{6}$$

For every mole of $CaCO_3$ that dissolves, two moles of A_T are formed and one extra mole of DIC is generated from the $CaCO_3$. Therefore, the amount of DIC generated from $CaCO_3$ dissolution is half the amount of A_T increase between the inlet and outlet of the reactor.

In AWL applications, the critical quantity is the overall DIC increase resulting from net CO_2 sequestration, i.e., ΔDIC_{seq}. Here we need to make a distinction between the buffered and unbuffered scenario. In the unbuffered scenario, one calculates the DIC and A_T values after re-equilibration of the process water with the atmosphere

$$A_{T,final} = A_{T,outlet} = A_{T,inlet} + \Delta A_{T,carb} \tag{7}$$

$$DIC_{final} = f(A_{T,final}, pCO_{2,atm}) \approx DIC_{inlet} + \left(\frac{\partial DIC}{\partial A_T}\right)_{pCO_{2,atm}} \Delta A_{T,carb} \tag{8}$$

The A_T concentration does not change during re-equilibration (remains same as the outlet), while the final DIC value can be calculated from this A_T concentration and the atmospheric pCO_2 based on thermodynamic relations of seawater carbonate chemistry (assuming full equilibration with the atmosphere). The approximation in Eq. (9) uses the thermodynamic buffer factor $\gamma = \left(\partial DIC / \partial A_T\right)_{pCO_{2,atm}}$, which specifies the increase in seawater DIC taken due to CO_2 uptake from the atmosphere given a certain addition of alkalinity (Zeebe and Wolf-Gladrow, 2001). This buffer factor is calculated at the atmospheric pCO_2 and ambient seawater concentrations (i.e., inlet conditions), which serves as a reasonable approximation, since the outlet water will be quickly mixed with ambient seawater. Accordingly, in the unbuffered scenario, the total amount of CO_2 sequestered becomes:

$$\Delta DIC_{seq}^{unbuf} = DIC_{final} - DIC_{inlet} - \Delta DIC_{carb} = (2\gamma - 1)\Delta DIC_{carb} \tag{9}$$

The amount of CO_2 that is lost via outgassing upon re-equilibration can be calculated as:

$$\Delta DIC_{outgas} = DIC_{outlet} - DIC_{final} \tag{10}$$

In the case of buffered AWL, one adds additional alkalinity to the effluent water, until the equilibrium is reached with the ambient atmosphere, and so no CO_2 will be outgassed to the atmosphere. The final state is calculated as:

$$DIC_{final} = DIC_{outlet} \tag{11}$$

$$A_{T,final} = f(DIC_{outlet}, pCO_2^{atm}) \approx A_{T,inlet} + \frac{1}{\gamma}\left(DIC_{outlet} - DIC_{intlet}\right) \tag{12}$$

The final alkalinity value is again calculated from thermodynamic relations of seawater carbonate chemistry. The amount of alkalinity that needs to be supplied by liming to achieve "full buffering" is given by:

$$\Delta A_{T,buffer} = A_{T,final} - A_{T,inlet} - \Delta A_{T,carb} = \frac{1}{\gamma}\left(DIC_{outlet} - DIC_{intlet}\right) - \Delta A_{T,carb} \tag{13}$$

Accordingly, in the buffered scenario, the total amount of CO_2 sequestered can be calculated as:

$$\Delta DIC_{seq} = DIC_{outlet} - DIC_{inlet} - \Delta DIC_{carb} \tag{14}$$

The amount of CO_2 sequestration that is generated by buffering can be calculated as

$$\Delta DIC_{seq}^{buf} = \Delta DIC_{seq} - \Delta DIC_{seq}^{unbuf} \tag{15}$$

In our example (Table 1), the total DIC increase in the equilibrated effluent water amounts to $\Delta DIC_{total} = 0.25$ mM in the unbuffered case, of which 76 % (0.19 mM) originates from $CaCO_3$ dissolution and 24% (0.06 mM) is due to CO_2 sequestration from the flue gas. In the buffered case, the DIC increase in the buffered discharge water amounts to $\Delta DIC_{total} = 1.02$ mM of which 19% (0.19 mM) originates from $CaCO_3$ dissolution, 6% (0.06 mM) is due to unbuffered CO_2 sequestration and 75% (0.77 mM) results from additional (buffered) CO_2 sequestration via liming. This illustrates that in the unbuffered scenario, a large fraction of the CO_2 initially sequestered from the flue gas escapes back to the atmosphere upon release of the reactor water into the ocean.

The operation and performance of an AWL reactor can be quantified by introducing a number of efficiency factors, which can be calculated from the ΔDIC_{seq} and ΔDIC_{carb} values defined above (and hence from A_T and DIC values measured at the inlet and outlet of the reactor). The efficiency factors can again be linked to the different steps in the AWL process (as in Figure 2).

2.3. CO_2 sequestration efficiency and water usage

The key target of the AWL reactor is to remove CO_2 from the gas stream and store this permanently as DIC in the surface ocean. This performance is quantified by the CO_2 sequestration efficiency (η_{seq}), which is defined as the fraction of CO_2 sequestered from the gas stream, accounting for re-equilibration with the atmosphere and associated CO_2 degassing and buffering:

$$\eta_{seq} = \frac{\Delta DIC_{seq} RT}{\left(pCO_{2,gas} - pCO_{2,atm}\right)} \frac{Q_w}{Q_g} \tag{16}$$

In this, the reactor is fed with a gas stream Q_g ($m^3 s^{-1}$) at a certain CO_2 partial pressure ($pCO_{2,gas}$), and uses a process water stream Q_w ($m^3 s^{-1}$) which is characterized by DIC_{inlet} and $A_{T,inlet}$. R is the ideal gas constant (L atm $mol^{-1} K^{-1}$) and T is the temperature of the gas stream (K). The maximum CO_2 sequestration efficiency is achieved when upon exit, the process water is in full equilibrium with the flue gas and all the dissolved CO_2 in the process water is suitably buffered by $CaCO_3$ dissolution in the AWL reactor and/or additional buffering by liming, i.e., $\Delta DIC_{seq}^{\max} = DIC_{eq} - DIC_{inlet}$.

$$\eta_{seq}^{\max} = \frac{\left(DIC_{eq} - DIC_{inlet}\right)RT}{\left(pCO_{2,gas} - pCO_{2,atm}\right)}\frac{Q_w}{Q_g} \tag{17}$$

The equilibrium value, $DIC_{eq}\left(A_T^{inlet}, pCO_{2,gas}, T, S\right)$ can be calculated from carbonate chemistry as a function of the A_T of the inlet water and the pCO_2 of the gas stream. From this, the minimum water to gas flow ratio ($Q_{water,\min}/Q_{gas}$) that is required to achieve 100% CO_2 sequestration efficiency ($\eta_{seq}^{\max} = 1$) can be calculated as:

$$\frac{Q_{w,\min}}{Q_g} = \frac{(pCO_{2,gas} - pCO_{2,atm})}{RT(DIC_{eq} - DIC_{inlet})} \tag{18}$$

In our example reactor, this minimum water to gas flow ratio amounts to $Q_{water,\min}/Q_{gas}$ = 0.76 (Table 2). A water efficiency factor (W_{eff}) can be defined as actual water consumption of the reactor over the minimum required water flow to achieve maximum sequestration.

$$W_{eff} = \frac{Q_w}{Q_{w,\min}} \tag{19}$$

If W_{eff} is smaller than 1, the water flow is not sufficient to dissolve all the CO_2 in the gas stream down to atmospheric pCO_2 and so the sequestration efficiency is limited by the water flow rate ($\eta_{seq}^{\max} < 1$). If the W_{eff} is larger than 1, more water is used than is strictly required. In our example reactor, the maximum CO_2 uptake efficiency is 100% and W_{eff} = 3.2 (Table 2). The volume of process water (m^3) that is used to capture one tonne of CO_2 can be calculated from Eq. (17) as:

$$V_{water} = \frac{1}{\Delta DIC_{seq}}\frac{10^6}{M_{CO_2}} \tag{20}$$

In this, M_{CO2} is the molar mass of CO_2 (44.01 g mol^{-1}) and 10^6 is used to convert g to tonnes (1 g = 10^{-6} ton), while ΔDIC_{seq} is expressed in mol per unit of volume. In our reactor example, 150.000 m^2 of process water is used to capture 1 tonne of CO_2, thus illustrating the large water footprint of AWL.

2.4. CO_2 dissolution efficiency and $CaCO_3$ dissolution efficiency

In reality, the maximum CO_2 sequestration efficiency will not be reached, due to several forms of inefficiency. In the first step, there might be incomplete dissolution of CO_2 in the inlet water from the flue gas stream. To account for this, the **CO_2 dissolution efficiency** is defined as the amount of CO_2 that is effectively removed from the gas stream versus its theoretical maximum

$$\varepsilon_{CO_2} = \frac{DIC_{outlet} - DIC_{inlet} - \Delta DIC_{carb}}{DIC_{eq} - DIC_{inlet}} \tag{21}$$

The maximum CO_2 dissolution efficiency of 100% is reached when $DIC_{outlet} = DIC_{eq} + \Delta DIC_{carb}$. The CO_2 uptake efficiency is defined as the relative amount of CO_2 that is stripped from the incoming gas stream (irrespective of whether it is eventually sequestered or not – see below)

$$\eta_{uptake} = \varepsilon_{CO_2}\eta_{seq}^{\max} \tag{22}$$

As can be seen, the CO_2 uptake efficiency is critically dependent on the CO_2 dissolution efficiency ε_{CO_2} as well as the Q_{water}/Q_{gas} ratio at which the reactor operates (which defines $\eta_{seq}^{\max}$). In the example reactor, the CO_2 uptake efficiency (η_{uptake}) becomes 33%, implying that only a third of the CO_2 is removed from the gas stream.

In a second step, the dissolution of $CaCO_3$ in the AWL reactor targets the neutralization the dissolved CO_2 by its conversion to HCO_3^- via reaction Eq. (1). The **$CaCO_3$ dissolution efficiency** is defined as the percentage of the dissolved CO_2 within the reactor that has reacted with the carbonate minerals.

$$\varepsilon_{CaCO_3} = \frac{\Delta DIC_{carb}}{DIC_{outlet} - \Delta DIC_{carb} - DIC_{inlet}} \tag{23}$$

The maximum $CaCO_3$ dissolution efficiency is reached when the DIC released during carbonate dissolution matches the amount of CO_2 extracted from the gas phase, i.e., $\Delta DIC_{carb} = 1/2\left(DIC_{outlet} - DIC_{inlet}\right)$. In the example reactor, $CaCO_3$ dissolution efficiency is 22%, implying that only a part of the CO_2 extracted from the gas stream is buffered by $CaCO_3$ dissolution.

2.5. Outgassing and buffering effects

The outgassing effect ε_{outgas} is defined as the amount of amount of CO_2 sequestered in the unbuffered scenario relative to the amount of CO_2 that has reacted with the carbonate

$$\varepsilon_{outgas} = \frac{\Delta DIC_{seq}^{unbuf}}{\Delta DIC_{carb}} = (2\gamma - 1) \tag{24}$$

As shown in Eq. (9), the outgassing effect ε_{outgas} is directly proportional to the thermodynamic buffer factor γ, which is always smaller than 1, and so $\varepsilon_{outgas} < 1$. Finaly, the buffering effect is defined as:

$$\varepsilon_{buffer} = \frac{\Delta DIC_{seq}^{buf}}{\Delta DIC_{seq}^{unbuf}} = \frac{\Delta DIC_{seq}}{\Delta DIC_{seq}^{unbuf}} - 1 \tag{25}$$

Based on the factors introduced above, the effective CO_2 sequestration efficiency thus becomes:

$$\eta_{seq} = \frac{\Delta DIC_{seq} RT}{\left(pCO_{2,gas} - pCO_{2,atm}\right)} \frac{Q_{water}}{Q_{gas}} = \varepsilon_{CO_2}\varepsilon_{CaCO_3}(2\gamma - 1)\left[1 + \varepsilon_{buffer}\right]\eta_{seq}^{\max} \tag{26}$$

When there is no buffering ($\varepsilon_{buffer} = 0$) then $\eta_{seq} = \varepsilon_{CO_2}\varepsilon_{CaCO_3}(2\gamma - 1)\eta_{seq}^{\max}$. In contrast, when there is maximum buffering $\eta_{seq} = \varepsilon_{CO_2}\eta_{seq}^{\max} = \eta_{uptake}$, the CO_2 uptake efficiency is always the same as the CO_2 sequestration efficiency. In this scenario, the buffering compensates entirely for incomplete carbonate dissolution and prevents outgassing (i.e., $\varepsilon_{buffer} = \left[1 - \varepsilon_{CaCO_3}(2\gamma - 1)\right] / \left[\varepsilon_{CaCO_3}(2\gamma - 1)\right]$). In our example reactor, the unbuffered CO_2 sequestration efficiency is only 6% (see Table 2), while the buffered CO_2 sequestration efficiency (or equally, the CO_2 uptake efficiency) amounts to 33%, thus indicating that a large part of the CO_2 initially gained will be lost by outgassing upon re-equilibration.

3. Different reactor designs for AWL

Over the past decades, several reactor designs have been proposed for AWL. Some have remained at a conceptual model stage, while others have been tested in bench-top or pilot scale operations (Table 2). As such, the technological readiness level is still limited and restricted to pilot scale applications (Chou et al., 2015; Kirchner et al., 2020b). In this section, we will compare four different reactor designs: a one-step reactor (Caldeira and Rau, 2000; Chou et al., 2015), a two-step reactor (Chou et al., 2015), a slurry reactor (Kirchner et al., 2020b) and a buffered AWL reactor (Caserini et al., 2021). The operational conditions and process efficiencies of these reactor designs are summarized in Table 2.

Table 2: Operational and process conditions for a one- and two-step reactor (Chou et al., 2015), a slurry reactor (Kirchner et al., 2020b) and a BAWL reactor (Caserini et al., 2021). * = after the dissolution reactor, ** = after the buffering reactor as no degassing takes place. When water and/or gas flow rates are not specified, no CO_2 uptake or sequestration efficiency can be calculated, as was the case for Two-Step and BAWL.

		One-step	Two-step	Slurry	BAWL
Operational conditions	Operational stage	Bench-top	Bench-top	Pilot	Conceptual
	pCO_2 of the gas stream (atm)	0.15	0.15	0.10 – 0.12	0.28
	water/gas flow ratio (v/v)	3.5	2.6	0.3	/
	Min. water/gas flow ratio (v/v)	0.76	0.76	0.75	0.92
	Carbonate particle size (µm)	250 – 500	250 – 500	4	10
Process efficiency	Max sequestration efficiency (%)	100	100	40	/
	CO_2 dissolution efficiency (%)	57	33	63	93
	CO_2 uptake efficiency (%)	57	33	25	/
	$CaCO_3$ dissolution efficiency (%)	1	22	48	59
	CO_2 sequestration efficiency (%)	0.6	6	8	/
	pH before/after degassing	6.4/8.1	6.6/8.2	6.7/8.5	6.6*/8.0**
	Water efficiency factor	4.6	3.2	0.4	/
	Volume of water used per ton of CO_2 captured (10^3 m^3)	2000	150	17	2

3.1. One-step fixed-bed reactor

The first AWL reactor design comprised a one-step fixed-bed reactor (Fig. 3a), of which the theoretical concept was first presented in Rau and Caldeira (1999), and experimental results from a bench-top version were reported in Rau (2011). This reactor contains a porous bed of limestone particles, sprayed with water until they are submerged. The CO_2-rich gas enters through one or more inlets located at the bottom or lower half of the reactor (Fig. 3a). Subsequently, the gas stream passes over and through the wetted, porous bed of limestone particles, which then allows the CO_2 in the gas phase to hydrate in the pore fluid. The flue gas (partially) depleted in CO_2 leaves the reactor from the top and is discharged to the atmosphere.

As indicated by our analysis above, the CO_2 uptake from the gas is critically dependent on the water/gas flow rate Q_{water}/Q_{gas} - see Eq (22). This was confirmed by laboratory experiments with a bench-top version of the one-step fixed-bed reactor (Rau, 2011). At a low Q_{water}/Q_{gas} of below 1, the CO_2 uptake efficiency remained below ~30%, but could be increased up to 97% by increasing the water/gas (vol/vol) flow rate to >8. Chou et al. 2015 examined a similar lab-scale one-step reactor, and achieved a CO_2 uptake efficiency of ~57 % using a Q_{water}/Q_{gas} of 3.5 (Table 2). The dissolution of CO_2 in the process water generates a low-pH carbonic acid solution which then can react with the carbonates to form Ca^{2+} and HCO_3^-. The removal of CO_2 from the flue gas alone however does not imply that the reaction with limestone is completed. Rau (2011) found that the majority of the hydrated CO_2 did not react with the carbonate particles, and would be outgassed again to the atmosphere upon release. This was confirmed by a lab-scale one-step reactor investigated by Chou et al. (2015), which showed a very low $CaCO_3$ dissolution efficiency of ~1 % (Table 2). Consequently, the overall CO_2 sequestration efficiency of a one-step reactor remains low due the lack of conversion from hydrated CO_2 to HCO_3^-. The unreacted hydrated CO_2 will escape if the solution is exposed to the atmosphere during the re-equilibration step (Rau, 2011; Chou et al., 2015). With such a low $CaCO_3$ dissolution efficiency, the reactor configuration of Chou et al. (2015) requires an excessive ~2 million m^3 of water to sequester 1 tonne of CO_2 (Table 2). Possibilities to improve the $CaCO_3$ dissolution efficiency are to increase the reaction time or to decrease the limestone particle size as to increase the reactive surface area and dissolution rate (Rau, 2011).

3.2. Two-step reactor

A fundamental problem of a one-step reactor is that the reaction time of CO_2 dissolution is much faster than that of $CaCO_3$ dissolution, thus leading to a low $CaCO_3$ dissolution efficiency. To accommodate this, a two-step reactor design was tested to improve the $CaCO_3$ dissolution efficiency (Chou et al., 2015). In this, the dissolution of CO_2 in the process water, and the $CaCO_3$ dissolution occur in two separated reactors placed in series (Fig. 3b). In the first step, the CO_2-rich gas stream is brought into contact with the inlet process water in a gas-liquid reactor, and after the pH of the process water is stabilized, the acid solution is fed into a liquid-solid reactor filled with limestone powder (>95 wt.% $CaCO_3$) with a particle size of 250 – 500 µm (Chou et al., 2015). Under identical operation conditions, the $CaCO_3$ dissolution efficiency could be increased from 1% in the one-step process to 22% in the two-step process (Chou et al., 2015). This strongly reduces the required amount of water needed to sequester 1 tonne of CO_2 to ~150.000 m^3 (Chou et al., 2015).

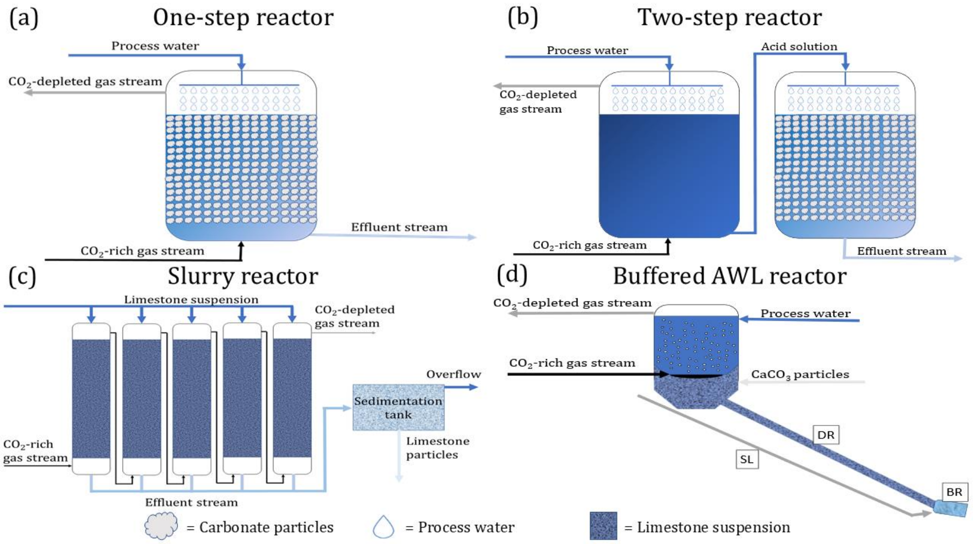

Figure 3: Conceptual reactor design of four AWL reactors. (a) One-step reactor, (b) Two-step reactor, (c) Slurry reactor, (d) Buffered AWL reactor. SL = slaked lime pipe, DR = dissolution reactor, BR = buffering reactor.

3.3. Slurry reactor

The next improvement in reactor design was achieved by using a suspension of fine $CaCO_3$ instead of a reactor with large $CaCO_3$ grains (Fig. 3c). This reactor design was implemented in an AWL demonstration plant at a coal-fired power plant in Wilhelmshaven (Germany) that could process up to 200 m^3 h^{-1} of flue gas (Kirchner et al., 2020b). The AWL reactor consisted of a five columns of 1.95 m high and 0.32 m in diameter packed with plastic packing rings to increase the surface area within the reactor to enhance the dissolution of CO_2 into the water as well as the subsequent $CaCO_3$ dissolution. A limestone suspension of approximately 0.5% (w/w) was sprayed into the head space of each column. The desulfurized flue gas from the coal-fired power plant entered the columns from the bottom side. The flue gas was channeled through all five columns sequentially to achieve maximal removal of CO_2. The flue gas leaving the last column was fed back into the chimney of the power plant. These improvements resulted in a CO_2 uptake efficiency of 15 to 55% during the operation of this AWL demonstration plant with the uptake efficiency being inversely proportional to the gas flow rate. For a water/gas flow rate of 0.3, a CO_2 uptake efficiency of 25% was achieved (Table 2; Kirchner et al., 2020b). At this Q_{water}/Q_{gas}, the W_{eff} is smaller than 1 and the water flow rate limits the maximum achievable CO_2 sequestration efficiency (η_{seq}^{max} = 40%). The CO_2 uptake efficiency can be further improved by increasing the water/gas flow rate, by increasing the number of reactor columns or by recirculating the gas stream. Note however that all these factors lead to a larger (and hence more costly) reactor setup.

The $CaCO_3$ dissolution, step (ii), was improved by using a limestone suspension with micronized carbonate particles (~4µm) and by improving mixing and turbulence within the reactor by implementation of the plastic packing rings (Kirchner et al., 2020b). This resulted in an A_T increase from 2 mM in the input stream to 5.6 mM in the effluent water and a $CaCO_3$ dissolution efficiency of 48% (Table 2; Kirchner et al., 2020b). This resulted in a substantially reduced water consumption (17.000 m^3 per ton of CO_2 sequestered) compared to the one-step and two-step reactors (Table 2; Kirchner et al., 2020b). When the process was performed in a closed-loop with

https://doi.org/10.5194/egusphere-2025-447
Preprint. Discussion started: 13 February 2025

recirculation of the process water, an A_T of >10 mM was achieved. This indicated that the contact time between the limestone suspension and the flue gas was too short in the one-pass setup. Additional columns, elongation of the existing ones, and higher limestone concentrations could be considered for optimization of the reactor design (Kirchner et al., 2020b). The solution leaving the columns was fed into a sedimentation tank to separate the remaining limestone particles from the process water. The particle-poor overflow water was then fed into the wastewater treatment system of the powerplant (Kirchner et al., 2020b).

3.4. Buffered accelerated weathering of limestone (BAWL) reactor

The feasibility of unbuffered AWL reactors is limited by the large water requirements (10^3 – 10^5 m^3 water per ton of CO_2 sequestered) in current reactor designs (Rau and Caldeira, 1999; Rau, 2011; Caserini et al., 2021). This large water requirement is a direct consequence of the low $CaCO_3$ dissolution efficiency ε_{CaCO_3} (as illustrated by Eq. 24-25). To increase the $CaCO_3$ dissolution efficiency, longer reaction times and thus larger reactors are required, which then also increases capital investment (Rau, 2011; Kirchner et al., 2020b). A second issue of unbuffered AWL reactors, is the outgassing effect ε_{outgas}. If the effluent solution is exposed to the atmosphere, excess CO_2 will be degassed until the effluent is in equilibrium with the pCO_2 of the ambient atmosphere. One option would be to avoid contact with the atmosphere. If the effluent would be directly discharged into the deep sea, the CO_2 storage potential is higher as it avoids extensive degassing. However, this would lead to acidification of the deeper ocean and associated environmental impacts (Caserini et al., 2021).

To overcome the issues of low $CaCO_3$ dissolution efficiency, high water requirements and inefficient CO_2 sequestration of unbuffered AWL, the concept of "buffered AWL" has been proposed (Caserini et al., 2021). Buffered AWL (BAWL) reactors have not been physically built or tested, and still reside within the conceptual phase. Buffered AWL consists of four distinct sections: a mixer, a dissolution reactor (DR), slaked lime pipe (SL) and a buffering reactor (BR) (Fig. 3d). The main difference between AWL is the buffering of the unreacted CO_2 by $Ca(OH)_2$. In the mixer, CO_2 from the gas stream is mixed with seawater and carbonate particles to form a homogeneous slurry. The CO_2 gas stream enters the mixer from the bottom and is hydrated through a bubble-type absorption column or a packed bed absorption column. A bubble type absorption column would be preferred as the absorption can be 3 – 10 times faster than in a packed bed column, which reduces the reactor size significantly (Teir et al., 2014; Xing et al., 2022; Zhang et al., 2023). The CO_2-depleted gas is released at the top of the mixer. Seawater is fed to the mixer from the upper part. This theoretical example assumes a dissolution of 1000 kg of CO_2 in 2000 m^3 process water, at which point the process water is in equilibrium with the flue gas ($pCO_2 \cong 0.28$ bar) (Caserini et al., 2021).

Carbonate mineral particles, with a suitably small diameter (<50 μm) so that they remain in suspension, are uniformly mixed with the main water stream at the bottom of the mixer before entering into the dissolution reactor (DR). The dissolution rate of the carbonate particles is determined by the size of the carbonate particles, residence time and pressure in the dissolution reactor (Caserini et al., 2021). The primary objective of the DR is to maximize the amount of dissolved carbonate mineral per ton of absorbed CO_2 in solution (Caserini et al., 2021). The DR consists of a piping system in which the carbonate minerals are dissolved into a fully ionic solution during transport to the coastal ocean. The DR can be located both on- and offshore. If the DR is constructed offshore, between the coasts and the deeper ocean, the solution flowing down the DR encounters increasing the hydrostatic pressure which improves the dissolution of the carbonate minerals (Dong et al., 2018; Caserini et al., 2021). The carbonate dissolution efficiency (step (ii)) of this theoretical example was 59% (Table 2). The solution leaving the DR will be acidic as CO_2 needs to be present in stoichiometric excess to allow full dissolution of the carbonate particles. Therefore, a final buffering in the buffering reactor (BR) is needed before discharge to the ocean. This BR is located at the end of the DR. Aqueous calcium hydroxide ($Ca(OH)_2$), supplied through the slaked lime pipe, is mixed with the acid solution leaving the DR. The $Ca(OH)_2$ reacts with the unreacted CO_2 remaining in the solution at the end of the DR.

The buffering of the unreacted CO_2 by $Ca(OH)_2$ allows to release an ionic solution at the same pH as the seawater and thereby avoiding acidification. The buffering also avoids degassing of the unreacted CO_2 and increases the long-term storage efficiency of the process compared to traditional AWL (Caserini et al., 2021; Chou et al., 2015; Rau, 2011). The use of a tubular reactor in the BAWL process also allows for long residence times, higher pressures and reduces the need for maintenance. High-density poly-ethylene (HDPE) pipelines have a long life-time and can be used up to 900 m deep. Extending the DR into the deep sea allows for efficient dissolution of carbonates as dissolution is favored at high pressure. This reduces the amount of $Ca(OH)_2$ that would be needed to compensate for the unreacted CO_2 left in the solution.

The use of $Ca(OH)_2$ and micronized carbonate particles comes, however, at an energy and CO_2 penalty. This penalty can be minimized by using electric energy from renewable sources for the production of $Ca(OH)_2$ and the milling of carbonate minerals (Caserini et al., 2021). Furthermore, $Ca(OH)_2$ can potentially be made from steel slags at low temperatures lowering the CO_2 emissions by at least 65% (Castaño et al., 2021). The estimated cost for capturing and storing CO_2 using BAWL is comparable with estimates for large-scale geological carbon capture and storage projects (De Marco et al., 2023).

4. AWL feedstocks

The three feedstock components needed for traditional AWL are water, limestone ($CaCO_3$) carbonate, and CO_2, with the addition of calcium hydroxide ($Ca(OH)_2$) in the case of buffered AWL. The amount of materials needed will depend of the pCO_2 in the flue gas and the efficiency of the reactor (Table 2).

Limestone (containing 92 – 98% $CaCO_3$ (Rau et al., 2007)) is the primary mineral source of $CaCO_3$ as it is much more abundant and less expensive than pure $CaCO_3$ (~4$ ton^{-1} limestone, ~105$ ton^{-1} dolomite, ~400$ ton^{-1} pure $CaCO_3$; Calcium Carbonate Prices, News, Monitor, Analysis & Demand, 2024; Caserini et al., 2021). The US production of limestone was about 1.05 x10^{9} tons in 2023 (Survey, 2023), with Sweden being the largest producer in Europe accounting for a production of 6.3 x10^{6} tons in 2021 (Mineral statistics, 2024). About 20% of the limestone production and processing results in waste limestone fines with no significant market value (Rau et al., 2007). These fines could be used as a low-cost source of carbonate for application in AWL and at the same time reduce waste from limestone mining and processing.

Significant volumes of water are needed to dissolve the CO_2 and dilute the resulting bicarbonate in the original reactor designs (10^4 - 10^5 ton of water/ton CO_2; Table 2) (Rau et al., 2007; Rau and Caldeira, 1999), although more recent designs have reduced the water demand by a few orders of magnitude (~ 10^3 ton of water/ton CO_2; Table 2). The high water demand and the accompanying cost could limit the feasibility of the overall AWL process. Therefore, a low-cost water source such as cooling water from a power plant or other sources of recycled water should be used preferably. The use of seawater is also an attractive option as it is a virtually limitless source and bicarbonate-containing effluent could be directly dumped and diluted in the ocean after degassing or buffering and removal of potential contaminants (Rau and Caldeira, 1999).

https://doi.org/10.5194/egusphere-2025-447
Preprint. Discussion started: 13 February 2025

The third resource needed in the AWL process is CO_2. AWL can use different industrial point sources of CO_2. However, the CO_2 concentration in the flue gas of different industrial sources can vary substantially from 3 to 4 vol% in a natural gas turbine up to 25 vol% in cement plants (De Marco et al., 2023). As increased CO_2 concentrations in the gas stream promotes dissolution of CO_2 in the seawater, industrial sources with high concentrations of CO_2 in the flue gas are preferable (De Marco et al., 2023; Rau and Caldeira, 1999).

Buffered accelerated weathering of limestone (BAWL) uses a fourth feedstock, calcium hydroxide ($Ca(OH)_2$) also known as slaked lime. The $Ca(OH)_2$ is used to buffer the remaining unreacted CO_2 at the end of the reactor to be able to release a solution at the same pH as the seawater (Caserini et al., 2021). The BAWL reactor setup proposed by Caserini et al. consumes 0.4 tons of $Ca(OH)_2$ to store 1 ton of CO_2 (Caserini et al., 2021). Slaked lime is produced through calcination of limestone to form calcium oxide (CaO), which is then granulated and hydrated to from $Ca(OH)_2$ (Castaño et al., 2021). This production process generates about 1 ton of CO_2 per ton of $Ca(OH)_2$, which results in a large CO_2 penalty of 0.4 ton CO_2 per ton of CO_2 stored of the overall BAWL process. However, if $Ca(OH)_2$ can be made from alkaline industrial waste, such as steel slag, through a calcination-free pathway, the specific CO_2 intensity can be reduced by as much as 65% (Castaño et al., 2021). This will greatly improve the CO_2 sequestration efficiency of the BAWL process.

Due to the high resource requirements especially for process water and $CaCO_3$, the (B)AWL plant should preferably be located near the coast and close to limestone deposits and mines. This will reduce the economic and environmental cost of long distance transport of large volumes of water and limestone and thereby increase the overall efficiency of the (B)AWL process (Kirchner et al., 2021; Rau et al., 2007).

5. Environmental concerns

Seawater is the preferrable source of process water for AWL as it requires large volumes of water. The intake of large volumes of seawater could lead to entrainment and impingement of small marine organisms (Liyanaarachchi et al., 2014; Missimer and Maliva, 2018). To avoid additional environmental damage to marine organisms from seawater intake, downstream seawater discharge of cooling water from power plant facilities could be used. This combined water usage has several benefits which include: 1) avoidance of the need to build expensive offshore intake structures, 2) no need for maintenance of the offshore infrastructure, 3) avoid extra potential damage from seawater intake and 4) minimal need for environmental permitting as primary intake is already permitted (Liyanaarachchi et al., 2014).

During the process of AWL, large amounts of effluent water will be produced that needs to be discharged in rivers or coastal areas. As seawater is a preferred source of process water used in AWL, disposal of the effluent water in the ocean will be the most likely option. Considering the large pool of DIC already present in the ocean and the natural variability of alkalinity on diurnal, seasonal and interannual basis, the discharge of AWL effluent water can be expected to only have minor effect on A_T and DIC concentrations (Rau et al., 2007; Kirchner et al., 2020a). Nevertheless, changes in the balance between A_T and DIC induced by AWL discharge can affect pH and the calcite and aragonite saturation state ($\Omega_{calcite}/\Omega_{aragonite}$) (Chou et al., 2015; Kirchner et al., 2020a), which in turn can impact the calcification rate of several major groups of marine calcifiers such as coccolithophores, foraminifera and corals, in a similar fashion as ongoing ocean acidification (Kleypas et al., 1999; Ries et al., 2009). However, the pH in coastal ecosystem can vary strongly in space and time. In vegetated areas, photosynthesis and respiration cause significant change in the environmental pH on a diurnal time scale (0.2 – 0.7 pH units; Hendriks et al., 2014; Rivest and Gouhier, 2015; James et al., 2020), with the largest pH fluctuations found in sheltered areas with low hydrodynamics (James et al., 2020). Therefore, it is important to consider the local ecosystem and hydrodynamic regime to estimate the effect the discharge water will have on the local environment. The effluent pH from the reactors analyzed here are in the range 6.4 – 8.5 (Table 2). If the effluent with a pH of 6.5 were discharged directly into the ocean, the expect acidification impact would be significant. To limit environmental effects, the effluent could be diluted with seawater before discharge. A 10-fold dilution would be sufficient to bring an effluent pH of 6.5 back to within the tolerable range of < 0.2 pH units change from background levels (Chou et al., 2015). Discharge in a place with strong currents would be favorable to achieve rapid advection and mixing between the discharge water and the receiving seawater (Chou et al., 2015). Inversely, if the effluent water is allowed to equilibrated with the atmosphere before discharge, or buffered with $Ca(OH)_2$, the increased alkalinity and pH could potentially limit ocean acidification (Rau and Caldeira, 1999; Rau et al., 2007; Chou et al., 2015; Kirchner et al., 2020a).

Another environmental concern is the potential release of impurities from the limestone or flue gas. In particular if flue gas from coal-fired power plants would be used, as this is known to contain SO_x, NO_x and trace elements (Rau et al., 2007; Kirchner et al., 2020a, b). The dissolution of SO_x and NO_x can lead to the formation of strong acids such as H_2SO_4, HNO_3, and HNO_2. These dissolution products can lead to eutrophication and reduced biodiversity, if discharged directly in the aquatic environment. Existing flue gas desulfurization facilities already in use at most power plants can effectively remove most of the SO_x contained in the flue gas. The solubility of NO_x is fairly limited and most will leave with the CO_2-depleted gas stream leaving the AWL reactor. The effluent stream of an AWL pilot plant utilizing desulfurized flue gas contains SO_4^{2-} and N-species in concentrations below the marine background level (Kirchner et al., 2020b). Trace elements such as Ba, Co, Ni and Zn could be released from the flue gas or from the dissolution of the carbonate minerals, while increased concentrations of Mn and Co were found in the effluent stream of the AWL plant in Wilhelmshaven (Germany). However, the final concentrations were not expected to be of environmental concern and well below the environmental guidelines (Kirchner et al., 2020b).

The disposal of large volumes of process water enriched in A_T can potentially inhibit natural carbonate dissolution within the coastal sediment (Bach, 2024). Increasing the seawater alkalinity locally at the location of disposal can increase the Ω_{calc} to levels at which carbonate dissolution is lowered, inhibited or carbonate precipitation occurs. If this would occur, the efficiency of the AWL process would be reduced as the CO_2 sequestration by AWL would be partially compensated by a loss of natural CO_2 sequestration. Furthermore, large scale operations of AWL and other ocean alkalinization methods could potentially affect global levels of $CaCO_3$ over much longer timescales (Bach, 2024).

6. Summary and conclusions

Accelerated weathering of limestone (AWL) is a Carbon Capture and Storage (CCS) technology that aims to artificially increase the weathering rate of carbonate minerals (Rau and Caldeira, 1999). The AWL process consist of four main steps: (i) The CO_2 uptake step, (ii) the $CaCO_3$ dissolution step and (iii) the alkalinization step (for buffered AWL) and the re-equilibration step (iv).

Since the first AWL reactor design proposed by Rau and Caldeira in 1999 (Rau and Caldeira, 1999), laboratory experiments and pilot scale operations have optimized the CO_2 uptake efficiency and reduced resource consumption. Nevertheless, large quantities of water are still needed for the dissolution of $CaCO_3$, while degassing of CO_2 after contact of the effluent with the atmosphere limits the CO_2 sequestration efficiency. The concept of buffered AWL, as proposed by Caserini et al. (2021), reduces the water requirements and increases the CO_2 sequestration efficiency by adding an extra $Ca(OH)_2$ buffering step. This additional step however comes at a CO_2 penalty, as production of $Ca(OH)_2$ emits CO_2.

Intelligent design of reactors and generation of feedstock can further optimize the CO_2 sequestration efficiencies. The tubular reactor design used in BAWL reduces the required reactor size significantly compared to traditional AWL reactors. The use of a tubular reactor furthermore allows for long residence times and higher pressures which stimulates $CaCO_3$ dissolution (Caserini et al., 2021). Furthermore, using renewable energy and starting from waste limestone fines for the milling of carbonate particles and producing $Ca(OH)_2$ from alkaline industrial waste via calcination-free processes can avoid the CO_2 penalty of BAWL (Caserini et al., 2021; Castaño et al., 2021). The pumping of the large quantities of process water needed in (B)AWL require a significant amount of energy. Therefore, optimization of the water usage is needed and could be achieved by increasing the pressure of the incoming gas stream or increasing the fraction of CO in the gas stream. Reusing the cooling water from nearby power plant could further reduce costs and environmental damage associated with large water intake. Further optimization of the dissolution kinetics of the micronized carbonate particles could reduce the amount of $Ca(OH)_2$ needed in the buffering and thereby reducing the energy and CO_2 penalty from the $Ca(OH)_2$ production.

The effects of disposing large amounts of effluent with increased alkalinity, altered pH and trace elements to the marine environment are currently poorly constrained. Existing research on ocean acidification and ecotoxicological studies on trace element toxicity can provide information of ecosystem impacts of AWL water discharge. However, because of the limited number of operational pilot plants, little is known about the actual conditions that can be expected for AWL water discharge. If AWL is to be implemented as a CCS technology on a large scale in the next decade, more pilot plants should be constructed sooner rather than later.

Code availability

The code used for analysis in this study is available upon request. Interested parties may contact the corresponding author.

Author contribution

FJRM conceptualized the idea for the review. TH was responsible for data collection, analysis and visualisation and SJVDV supervised the study. TH and FJRM worked out the model formulation. TH has written the manuscript with substantial contribution from all authors.

Competing interests

The authors declare that they have no conflict of interest.

Financial support

This research was supported by the Research foundation Flanders (FWO-SBO project S000619N) and the VLAIO Blauwe cluster project “Blue Alkalinity” (HBC.2023.0496). Additional financial support was provided by Team for the Planet (https://team-planet.com), a citizen community initiative dedicated to tackling of the climate challenge (funding through a collaboration agreement with its Carbon Time subsidiary).

Acknowledgements

The authors thank Gunter Flipkens for academic discussions.

https://doi.org/10.5194/egusphere-2025-447
Preprint. Discussion started: 13 February 2025

References

Calcium Carbonate Prices, News, Monitor, Analysis & Demand: https://www.chemanalyst.com/Pricing-data/calcium-carbonate-1158, last access: 27 March 2024.

Mineral statistics: https://www.sgu.se/en/mineral-resources/mineral-statistics/, last access: 27 March 2024.

Bach, L. T.: The additionality problem of ocean alkalinity enhancement, Biogeosciences, 21, 261–277, https://doi.org/10.5194/bg-21-261-2024, 2024.

Berner, R. A. and Berner, R. A.: The Phanerozoic Carbon Cycle: CO2 and O2, Oxford University Press, Oxford, New York, 158 pp., 2004.

Berner, R. A. and Morse, J. W.: Dissolution kinetics of calcium carbonate in sea water; IV, Theory of calcite dissolution, American Journal of Science, 274, 108–134, 1974.

Berner, R. A., Lasaga, A. C., and Garrels, R. M.: The Carbonate-Silicate Geochemical Cycle and Its Effect on Atmospheric Carbon-Dioxide over the Past 100 Million Years, Am J Sci, 283, 641–683, https://doi.org/10.2475/ajs.283.7.641, 1983.

Caldeira, K. and Rau, G. H.: Accelerating carbonate dissolution to sequester carbon dioxide in the ocean: Geochemical implications, Geophysical Research Letters, 27, 225–228, https://doi.org/10.1029/1999GL002364, 2000.

Calvin, K., Dasgupta, D., Krinner, G., Mukherji, A., Thorne, P. W., Trisos, C., Romero, J., Aldunce, P., Barrett, K., Blanco, G., Cheung, W. W. L., Connors, S., Denton, F., Diongue-Niang, A., Dodman, D., Garschagen, M., Geden, O., Hayward, B., Jones, C., Jotzo, F., Krug, T., Lasco, R., Lee, Y.-Y., Masson-Delmotte, V., Meinshausen, M., Mintenbeck, K., Mokssit, A., Otto, F. E. L., Pathak, M., Pirani, A., Poloczanska, E., Pörtner, H.-O., Revi, A., Roberts, D. C., Roy, J., Ruane, A. C., Skea, J., Shukla, P. R., Slade, R., Slangen, A., Sokona, Y., Sörensson, A. A., Tignor, M., Van Vuuren, D., Wei, Y.-M., Winkler, H., Zhai, P., Zommers, Z., Hourcade, J.-C., Johnson, F. X., Pachauri, S., Simpson, N. P., Singh, C., Thomas, A., Totin, E., Arias, P., Bustamante, M., Elgizouli, I., Flato, G., Howden, M., Méndez-Vallejo, C., Pereira, J. J., Pichs-Madruga, R., Rose, S. K., Saheb, Y., Sánchez Rodríguez, R., Ürge-Vorsatz, D., Xiao, C., Yassaa, N., Alegría, A., Armour, K., Bednar-Friedl, B., Blok, K., Cissé, G., Dentener, F., Eriksen, S., Fischer, E., Garner, G., Guivarch, C., Haasnoot, M., Hansen, G., Hauser, M., Hawkins, E., Hermans, T., Kopp, R., Leprince-Ringuet, N., Lewis, J., Ley, D., Ludden, C., Niamir, L., Nicholls, Z., Some, S., Szopa, S., Trewin, B., Van Der Wijst, K.-I., Winter, G., Witting, M., Birt, A., Ha, M., et al.: IPCC, 2023: Climate Change 2023: Synthesis Report. Contribution of Working Groups I, II and III to the Sixth Assessment Report of the Intergovernmental Panel on Climate Change [Core Writing Team, H. Lee and J. Romero (eds.)]. IPCC, Geneva, Switzerland., Intergovernmental Panel on Climate Change (IPCC), https://doi.org/10.59327/IPCC/AR6-9789291691647, 2023.

Cao, X., Li, Q., Xu, L., and Tan, Y.: A review of in situ carbon mineralization in basalt, Journal of Rock Mechanics and Geotechnical Engineering, 16, 1467–1485, https://doi.org/10.1016/j.jrmge.2023.11.010, 2024.

Caserini, S., Cappello, G., Righi, D., Raos, G., Campo, F., De Marco, S., Renforth, P., Varliero, S., and Grosso, M.: Buffered accelerated weathering of limestone for storing CO2: Chemical background, International Journal of Greenhouse Gas Control, 112, 103517, https://doi.org/10.1016/j.ijggc.2021.103517, 2021.

Castaño, S. V., Plante, E. C. L., Shimoda, S., Wang, B., Neithalath, N., Sant, G., and Pilon, L.: Calcination-free production of calcium hydroxide at sub-boiling temperatures, RSC Adv., 11, 1762–1772, https://doi.org/10.1039/D0RA08449B, 2021.

Chou, W.-C., Gong, G.-C., Hsieh, P.-S., Chang, M.-H., Chen, H.-Y., Yang, C.-Y., and Syu, R.-W.: Potential impacts of effluent from accelerated weathering of limestone on seawater carbon chemistry: A case study for the Hoping power plant in northeastern Taiwan, Marine Chemistry, 168, 27–36, https://doi.org/10.1016/j.marchem.2014.10.008, 2015.

De Marco, S., Varliero, S., Caserini, S., Cappello, G., Raos, G., Campo, F., and Grosso, M.: Techno-economic evaluation of buffered accelerated weathering of limestone as a CO2 capture and storage option, Mitig Adapt Strateg Glob Change, 28, 17, https://doi.org/10.1007/s11027-023-10052-x, 2023.

Dickson, A. G.: An Exact Definition of Total Alkalinity and a Procedure for the Estimation of Alkalinity and Total Inorganic Carbon from Titration Data, Deep-Sea Res, 28, 609–623, https://doi.org/10.1016/0198-0149(81)90121-7, 1981.

Dong, S., Subhas, A. V., Rollins, N. E., Naviaux, J. D., Adkins, J. F., and Berelson, W. M.: A kinetic pressure effect on calcite dissolution in seawater, Geochimica et Cosmochimica Acta, 238, 411–423, https://doi.org/10.1016/j.gca.2018.07.015, 2018.

Gadikota, G.: Carbon mineralization pathways for carbon capture, storage and utilization, Commun Chem, 4, 1–5, https://doi.org/10.1038/s42004-021-00461-x, 2021.

Hartmann, J., West, A. J., Renforth, P., Köhler, P., De La Rocha, C. L., Wolf-Gladrow, D. A., Dürr, H. H., and Scheffran, J.: Enhanced chemical weathering as a geoengineering strategy to reduce atmospheric carbon dioxide, supply nutrients, and mitigate ocean acidification, Rev Geophys, 51, 113–149, https://doi.org/10.1002/rog.20004, 2013.

Hendriks, I. E., Olsen, Y. S., Ramajo, L., Basso, L., Steckbauer, A., Moore, T. S., Howard, J., and Duarte, C. M.: Photosynthetic activity buffers ocean acidification in seagrass meadows, Biogeosciences, 11, 333–346, https://doi.org/10.5194/bg-11-333-2014, 2014.

Hofmann, A. F., Soetaert, K., Middelburg, J. J., and Meysman, F. J. R.: AquaEnv: An Aquatic Acid–Base Modelling Environment in R, Aquat Geochem, 16, 507–546, https://doi.org/10.1007/s10498-009-9084-1, 2010.

James, R. K., van Katwijk, M. M., van Tussenbroek, B. I., van der Heide, T., Dijkstra, H. A., van Westen, R. M., Pietrzak, J. D., Candy, A. S., Klees, R., Riva, R. E. M., Slobbe, C. D., Katsman, C. A., Herman, P. M. J., and Bouma, T. J.: Water motion and vegetation control the pH dynamics in seagrass-dominated bays, Limnology and Oceanography, 65, 349–362, https://doi.org/10.1002/lno.11303, 2020.

Kheshgi, H. S.: Sequestering atmospheric carbon dioxide by increasing ocean alkalinity, Energy, 20, 915–922, https://doi.org/10.1016/0360-5442(95)00035-F, 1995.

Kirchner, J. S., Lettmann, K. A., Schnetger, B., Wolff, J.-O., and Brumsack, H.-J.: Carbon capture via accelerated weathering of limestone: Modeling local impacts on the carbonate chemistry of the southern North Sea, International Journal of Greenhouse Gas Control, 92, 102855, https://doi.org/10.1016/j.ijggc.2019.102855, 2020a.

Kirchner, J. S., Berry, A., Ohnemüller, F., Schnetger, B., Erich, E., Brumsack, H.-J., and Lettmann, K. A.: Reducing CO2 Emissions of a Coal-Fired Power Plant via Accelerated Weathering of Limestone: Carbon Capture Efficiency and Environmental Safety, Environ. Sci. Technol., 54, 4528–4535, https://doi.org/10.1021/acs.est.9b07009, 2020b.

Kirchner, J. S., Lettmann, K. A., Schnetger, B., Wolff, J.-O., and Brumsack, H.-J.: Identifying Appropriate Locations for the Accelerated Weathering of Limestone to Reduce CO2 Emissions, Minerals, 11, 1261, https://doi.org/10.3390/min11111261, 2021.

Kleypas, J. A., Buddemeier, R. W., Archer, D., Gattuso, J.-P., Langdon, C., and Opdyke, B. N.: Geochemical Consequences of Increased Atmospheric Carbon Dioxide on Coral Reefs, Science, 284, 118–120, https://doi.org/10.1126/science.284.5411.118, 1999.

Liyanaarachchi, S., Shu, L., Muthukumaran, S., Jegatheesan, V., and Baskaran, K.: Problems in seawater industrial desalination processes and potential sustainable solutions: a review, Rev Environ Sci Biotechnol, 13, 203–214, https://doi.org/10.1007/s11157-013-9326-y, 2014.

Matter, J. M. and Kelemen, P. B.: Permanent storage of carbon dioxide in geological reservoirs by mineral carbonation, Nature Geosci, 2, 837–841, https://doi.org/10.1038/ngeo683, 2009.

Meysman, F. J. R. and Montserrat, F.: Negative CO emissions via enhanced silicate weathering in coastal environments, Biol Letters, 13, https://doi.org/10.1098/rsbl.2016.0905, 2017.

Missimer, T. M. and Maliva, R. G.: Environmental issues in seawater reverse osmosis desalination: Intakes and outfalls, Desalination, 434, 198–215, https://doi.org/10.1016/j.desal.2017.07.012, 2018.

Morse, J. W. and He, S.: Influences of *T*, *S* and *P*CO2 on the pseudo-homogeneous precipitation of CaCO3 from seawater: implications for whiting formation, Marine Chemistry, 41, 291–297, https://doi.org/10.1016/0304-4203(93)90261-L, 1993.

Morse, J. W., Arvidson, R. S., and Lüttge, A.: Calcium Carbonate Formation and Dissolution, Chem. Rev., 107, 342–381, https://doi.org/10.1021/cr050358j, 2007.

Mucci, A., Canuel, R., and Zhong, S.: The solubility of calcite and aragonite in sulfate-free seawater and the seeded growth kinetics and composition of the precipitates at 25°C, Chemical Geology, 74, 309–320, https://doi.org/10.1016/0009-2541(89)90040-5, 1989.

Rau, G. H.: CO2 Mitigation via Capture and Chemical Conversion in Seawater, Environ. Sci. Technol., 45, 1088–1092, https://doi.org/10.1021/es102671x, 2011.

Rau, G. H. and Caldeira, K.: Enhanced carbonate dissolution:: a means of sequestering waste CO2 as ocean bicarbonate, Energy Conversion and Management, 40, 1803–1813, https://doi.org/10.1016/S0196-8904(99)00071-0, 1999.

Rau, G. H., Knauss, K. G., Langer, W. H., and Caldeira, K.: Reducing energy-related CO2 emissions using accelerated weathering of limestone, Energy, 32, 1471–1477, https://doi.org/10.1016/j.energy.2006.10.011, 2007.

Renforth, P. and Henderson, G.: Assessing ocean alkalinity for carbon sequestration, Rev Geophys, 55, 636–674, https://doi.org/10.1002/2016rg000533, 2017.

Renforth, P. and Kruger, T.: Coupling Mineral Carbonation and Ocean Liming, Energy Fuels, 27, 4199–4207, https://doi.org/10.1021/ef302030w, 2013.

Ries, J. B., Cohen, A. L., and McCorkle, D. C.: Marine calcifiers exhibit mixed responses to CO2-induced ocean acidification, Geology, 37, 1131–1134, https://doi.org/10.1130/G30210A.1, 2009.

Rivest, E. B. and Gouhier, T. C.: Complex Environmental Forcing across the Biogeographical Range of Coral Populations, PLOS ONE, 10, e0121742, https://doi.org/10.1371/journal.pone.0121742, 2015.

Romanov, V., Soong, Y., Carney, C., Rush, G. E., Nielsen, B., and O'Connor, W.: Mineralization of Carbon Dioxide: A Literature Review, ChemBioEng Reviews, 2, 231–256, https://doi.org/10.1002/cben.201500002, 2015.

Sanderson, B. M., O'Neill, B. C., and Tebaldi, C.: What would it take to achieve the Paris temperature targets?, Geophys Res Lett, 43, 7133–7142, https://doi.org/10.1002/2016gl069563, 2016.

Snæbjörnsdóttir, S. Ó., Sigfússon, B., Marieni, C., Goldberg, D., Gislason, S. R., and Oelkers, E. H.: Carbon dioxide storage through mineral carbonation, Nat Rev Earth Environ, 1, 90–102, https://doi.org/10.1038/s43017-019-0011-8, 2020.

Song, Y., Jun, S., Na, Y., Kim, K., Jang, Y., and Wang, J.: Geomechanical challenges during geological CO2 storage: A review, Chemical Engineering Journal, 456, 140968, https://doi.org/10.1016/j.cej.2022.140968, 2023.

Survey, U. S. G.: Mineral commodity summaries 2023, Mineral Commodity Summaries, U.S. Geological Survey, https://doi.org/10.3133/mcs2023, 2023.

Teir, S., Suomalainen, M., and Onarheim, K.: Pre-evaluation of a new process for capture of CO2 using water, 2014.

Thonemann, N., Zacharopoulos, L., Fromme, F., and Nühlen, J.: Environmental impacts of carbon capture and utilization by mineral carbonation: A systematic literature review and meta life cycle assessment, Journal of Cleaner Production, 332, 130067, https://doi.org/10.1016/j.jclepro.2021.130067, 2022.

United Nations Environment Programme: Emissions Gap Report 2024: No more hot air … please! With a massive gap between rhetoric and reality, countries draft new climate commitments., United Nations Environment Programme, 2024.

Veetil, S. P. and Hitch, M.: Recent developments and challenges of aqueous mineral carbonation: a review, Int. J. Environ. Sci. Technol., 17, 4359–4380, https://doi.org/10.1007/s13762-020-02776-z, 2020.

Xing, L., Pullin, H., Bullock, L., Renforth, P., Darton, R. C., and Yang, A.: Potential of enhanced weathering of calcite in packed bubble columns with seawater for carbon dioxide removal, Chemical Engineering Journal, 431, 134096, https://doi.org/10.1016/j.cej.2021.134096, 2022.

Zeebe, R. E. and Wolf-Gladrow, D.: CO2 in seawater : equilibrium, kinetics and isotopes, Elsevier Science, Amsterdam, 2001.

Zhang, J., Yang, A., Darton, R., Xing, L., and Vaughan, A.: Surrogate modelling-assisted comparison of reactor schemes for carbon dioxide removal by enhanced weathering of minerals using seawater, Chemical Engineering Journal, 461, 141804, https://doi.org/10.1016/j.cej.2023.141804, 2023.